ELSEVIER

Chemical Engineering Science 61 (2006) 1819–1835

Chemical Engineering Science

www.elsevier.com/locate/ces

Liquid phase mixing in trayed bubble column reactors

Javier Alvaré[a,*], Muthanna H. Al-Dahhan[b]

[a]*Air Products and Chemicals Inc., 7201 Hamilton Blvd, Allentown, PA 18195, USA*
[b]*CREL, Washington University, Campus Box 1198, St. Louis, MO, 63130, USA*

Received 29 December 2004; received in revised form 23 September 2005; accepted 7 October 2005
Available online 1 December 2005

Abstract

The compartmentalization of conventional bubble columns by perforated trays constitutes a very effective method to reduce the liquid backmixing. The effect of tray design and operating conditions on the overall liquid mixing was studied in a bench-scale trayed bubble column. The extent of liquid backmixing in the column was investigated in light of liquid-phase tracer response experiments. In average, a three fold reduction in the liquid backmixing was achieved in the trayed column as compared to the column without the trays. Moreover, the tray open area and the superficial liquid velocity were found to have the strongest effects on the liquid backmixing. The N-CSTR with Backmixing Model was found to match the experimental tracer response curves better than the Axial Dispersion Model.

Keywords: Bubble column; Liquid backmixing; Multiphase reactor; Perforated trays; Compartment models; Axial dispersion model

1. Introduction

Bubble Columns are widely used as gas–liquid or gas–liquid–solid reactors in chemical, petrochemical, biotechnological and waste treatment industrial processes (Shah et al., 1982). Their advantages over other contacting devices are the simplicity of their construction and maintenance, low energy consumption, and minimal space requirements due to their vertical design.

Dudukovic et al. (1999), Joshi et al. (1998), and many others have reported the existence of a parabolic radial gas holdup profile in the operation of conventional bubble columns in the churn turbulent flow regime. This profile causes a difference in the density of the gas–liquid dispersion in the radial direction, with its maximum at the wall and its minimum at the center of the column. As a consequence of this radial density gradient, the liquid flows upwards in the central region of the column and downwards in the wall region. As a result, an intense axial liquid recirculation pattern sets in the column. Large axial backmixing is advantageous in processes that require good mass and heat transfer capabilities. However, it can also be a clear disadvantage due to the dilution of the reactants and products, which, in some cases, decreases the reaction driving force and hence reactor volumetric productivity and reactants conversion.

The sectionalization of conventional bubble columns by perforated trays into Trayed Bubble Columns has been demonstrated to be an efficient way to break the described gas–liquid phase macrocirculation pattern by creating independent mixed stages in between the trays (Patil et al., 1984; Joshi and Sharma, 1979; Schugerl et al., 1977). Several industrial processes such as the Visbreaking of petroleum residues (Palaskar et al., 2000) and the Fischer–Tropsch synthesis of liquid paraffins from syngas (Maretto and Krishna, 2000) can all benefit from the utilization of trayed bubble columns.

As opposed to single stage bubble columns, whose mixing characteristics have been extensively studied and reported in the scientific literature, far less studies have reported experimental and/or modeling work related to trayed bubble columns (Dudukovic et al., 1999; Palaskar et al., 2000; Vinaya and Varma, 1995; Blass and Cornelius, 1997). Many of the studies covered in the literature use conventional liquid-phase mixing model approaches to interpret the obtained experimental data and to quantify the effect of the different operating and/or design parameters studied. The axial dispersion model (ADM) has been traditionally used to describe and quantify the extent of liquid backmixing in different reactor systems. The

* Corresponding author. Tel.: +1 610 481 1357; fax: +1 610 706 7563.
E-mail address: alvarej@airproducts.com (J. Alvaré).

0009-2509/$ - see front matter © 2005 Elsevier Ltd. All rights reserved.
doi:10.1016/j.ces.2005.10.015

axial dispersion coefficient, which is the only parameter of the ADM, can be readily extracted from experiments (Palaskar et al., 2000; Magnussen and Schumacher, 1978). Multistage bubble columns are examples of contactors in which the flow of the phases seems to be properly represented by stagewise models such as the N-CSTR in series and the N-CSTR with backmixing models. In these models, the non-idealities of the liquid flow are described by the total number of mixed stages and the flowrates of the streams that connect them.

In spite of the efforts of the authors cited above, it is clear that a more exhaustive investigation of the effect of the controlling factors on the extent of the liquid phase backmixing is necessary to facilitate the design and operation of industrial scale co-current trayed bubble columns. In this work, tracer studies have been conducted in an experimental unit to study the effect of sectionalization on the overall liquid phase mixing in co-current trayed bubble columns. Furthermore, the ADM and the N-CSTR with backmixing models have been used to interpret the results of the experiments.

2. Literature review

It seems convenient to group the published work based on the models that the authors have chosen to interpret their experimental results. More often than not, the accuracy of the model interpretation of the experimental data is based upon the number of parameters that the model contains. Therefore, a balance between an adequate physical realization of the reactor system with a straightforward experimental verification must be sought when assessing the validity of a model. Simplified models can serve the purpose of providing us with a reasonable insight into the flow description without having to invest too much time and effort in the process.

One of the best known models is the ADM (Levenspiel, 1972). The model is the simplest mathematical description of a flow system in which both convection and diffusion are the governing transport mechanisms for backmixing. The diffusion term is modeled as a Fickian type process, in which both molecular and turbulent diffusion are lumped into a single diffusion coefficient, known as the axial dispersion coefficient, D_L. As for the convective transport term, the ADM assumes that any species in the system travels at the mean flow velocity. The dimensionless parameter, Peclet number, which represents the ratio of convective to diffusive mixing mechanisms, quantifies the extent of the liquid phase axial mixing. The ADM has been widely applied, due to the convenience of being able to describe the whole spectrum of backmixing states, from plug flow (absence of backmixing, $Pe =$ infinity) to perfect mixing ($Pe = 0$) with only one parameter. The number of empirical correlations developed for the axial dispersion coefficient in conventional bubble columns is very large (Myers, 1986). Table 1 provides a summary of published work, where the ADM has been used to explain liquid mixing in trayed bubble columns. In general, most of the reported findings are consistent about the effect of tray open area, tray hole diameter, tray spacing, and column diameter on the axial dispersion coefficient. The axial dispersion coefficient always increases with tray open area, tray hole diameter, tray spacing, and column diameter. It has unanimously been observed that there is no further reduction in the overall liquid backmixing when the diameter of the holes in the perforated trays is kept smaller than 5 mm. It has been reported that there is no dependency of superficial gas velocity on the liquid backmixing in counter-current trayed bubble columns (Vinaya and Varma, 1995). However, some discrepancies appear regarding the effect of superficial gas velocity in co-current columns. For instance, Ichikawa et al. (1967) reported a slight increase in the dispersion coefficient when the superficial gas velocity is smaller than 7 cm/s, after which point D_L rapidly increases until it reaches a maximum at 18 cm/s. On the other hand, other investigators (Palaskar et al., 2000; Chen and Yang, 1989) did not find the maximum reported by Ichikawa et al. (1967) but instead found a monotonic increase ($D_L \propto U_g^e$, $e = 0.12$–0.5), where the value of the exponent e is mainly a function of the operating regime.

Ichikawa et al. (1967) and Chen and Yang (1989) found a very weak effect of superficial liquid velocity on D_L, whereas other authors such as Schugerl et al. (1977), Vinaya (1994) and Palaskar et al. (2000) described a much more significant superficial liquid velocity effect ($D_L \propto U_l^{0.45\text{–}0.85}$). Palaskar et al. (2000) reported that the small effect of superficial liquid velocity, observed by the first group of investigators, was due to the fact that the order of magnitude of the generated liquid circulation velocity was significantly higher than the liquid superficial velocity (at least by a factor of 10). This order of magnitude difference masked the effect of the studied superficial liquid velocity. Dreher and Krishna (2001) estimated that the liquid circulation velocity in bubble columns without trays is about one order of magnitude higher than that measured in trayed bubble columns sectionalized by perforated trays of 18.6% open area. In addition, the authors reported that the axial dispersion coefficient increases with tray open area and that the diameter of the column has little effect on the extent of liquid backmixing.

In stagewise mixing models, the liquid backmixing is represented by a combination of individual interconnected stages of equal or different volumes. The connection between stages depends on the real reactor flow configuration. In addition to the main flow stream, we can also have bypass, recycle streams and/or dead volumes to simulate flow non-idealities. The applicability of these schemes ranges from the perfectly mixed to the plug flow situations. In the most general multistage models, single stages are considered to be perfectly mixed, although further non-idealities can be introduced to explain deviations from complete mixing behavior. The number of plausible model combinations is unlimited. However, one should always keep in mind that the advantages of any model are measured not only by how accurately it can describe the reactor behavior, but also by how specifically the model parameters can be experimentally estimated. Thus, the utilization of models containing more than two parameters should be avoided unless it is strictly necessary. The following is a survey of some of the multistage models that can be used to describe the overall liquid phase mixing in multistage bubble columns. The N-CSTR in series model is the simplest multistage model (Blass and Cornelius, 1997). It consists of a series of N equal and completely mixed

Table 1
Summary of surveyed published work the axial dispersion model is used to describe the liquid-phase mixing in trayed bubble columns

Reference	Gas–liquid arrangement	Apparatus and conditions	Correlation(s)	Main conclusions
Dreher and Krishna (2001)	Semi-batch	$H_c = 470, 370, 289$ cm $D_c = 10, 15, 38$ cm 2 perforated trays O.A. = 0.19%, 0.31% $d_0 = 0.05$ cm $U_g = 5$–40 cm/s	No correlations reported	Trays reduce liquid mixing in bubble column Backmixing increases with tray open area No effect of column diameter
Palaskar et al. (2000)	Co-current	$H_c = 77, 90$ cm; $D_c = 6.2, 20$ cm 3 perforated trays $H_S = 18, 20$ cm O.A. = 0.5%, 1.48%, 10.8% $d_0 = 0.32$ cm $U_g = 0.066$–0.2 cm/s $U_l = 0.0375$–0.075 cm/s	$\ln(Pe) = \left(\frac{T_i}{T}\right)^{-0.2}[0.023\ln^2(\mathrm{FP}) + 0.2658\ln(\mathrm{FP}) - 0.816]$ $\mathrm{FP} = \frac{U_g(\mathrm{O.A.})}{U_l}$ (Flow parameter) $Pe = \frac{U_l L}{D_L}$ (Peclet number)	$D_L \propto U_l^{0.45\text{–}0.85}$ $D_L \propto U_g^{0.12\text{–}0.2}$ Pe decreases with U_l and increases with U_g 20%–50% backmixing reduction when tray spacing is changed from 40 to 20 cm D_L depends on column diameter in the churn turbulent flow regime
Vinaya (1994)	Counter-current	$H_c = 180, 100$ cm $D_c = 9.8, 10, 54$ cm Perforated trays $H_S = 5, 12, 20, 85$ cm O.A. = 9.5%, 10%, 38%, 52% $d_0 = 0.3, 0.5, 1, 1.2$ cm $U_g = 1$–11 cm/s $U_l = 0$–2 cm/s	Bubbly flow: $Pe = 0.89\ U_l^{0.66}\mathrm{O.A.}^{-1.21} d_0^{0.3} H_S^{-0.6}$ $U_g = 0$–2.5 cm/s (valid range) Churn-turbulent flow: $Pe = 14\ U_l^{0.66}\mathrm{O.A.}^{-0.54} H_S^{-0.6}$ $U_g = 4$–10 cm/s (valid range)	
Chen and Yang (1989)	Co-current	$H_c = 120$ cm $D_c = 5, 7.5, 15$ cm 37 wire screen trays $H_S = 5$ cm O.A. = 64% $U_g = 0.2$–8 cm/s $U_l = 0$–3 cm/s	$D_L = 0.0094\ U_g^{0.5}$	D_L is independent of U_l D_L in trayed bubble columns is three orders of magnitude smaller thanin conventional bubble columns
Magnussen and Schumacher (1978)	Counter-current	$H_c = 400$ cm $D_c = 4, 100$ cm 2–16 sieve trays O.A. = 20% $d_0 = 1$ cm	No correlations reported	D_L decreases with an increase in the number of trays The effect of backmixing suppression due to the trays is stronger in columns with larger diameters
Ichikawa et al. (1967)	Counter-current	$H_c = 140, 188, 274$ cm $D_c = 4.7, 9, 13.7, 19.8$ cm Perforated trays O.A. = 10%–43.4% $d_0 = 1.5$–2 cm	$D_L = \mathrm{a(P/Dc)}^{0.8}\mathrm{S^K Dc}^{1.2} U_g^b$ $K = 0.967 U_g^{0.16}$ For $U_g = 1.4$–7.1 cm/s $a = 1.9$ and $b = 0.615$ For $U_g = 7$–18 cm/s $a = 0.64$ and $b = 1.2$	Effect on D_L of: U_l = Negligible U_g = Small increase for values < 7 cm/s, else very sensitive. Maximum at $U_g = 18$ cm/s d_0 = No effect for values > 0.5 cm, large decrease for $d_0 < 0.25$ cm $D_L \propto \mathrm{O.A.}^K$ $D_L \propto D_c^{0.4}$

Table 2
Summary of surveyed published work where the N-CSTR Model is used to describe the liquid-phase mixing in trayed bubble columns

Reference	Gas–liquid arrangement	Apparatus and conditions	Correlation(s)	Main conclusions
Blass and Cornelius (1997)	Co-current	$H_c = 325$ cm $D_c = 14$ cm 4 perforated trays $H_S = 53,\ 70$ cm O.A. = 1.1%–36% $d_0 = 0.2,\ 0.4$ cm $U_g = 1.5$–45 cm/s $U_l = 0.05$–1 cm/s	$\frac{N_{\text{eff}}}{N} = 1.061(\text{m/s})^{-0.19}\left(\frac{U_g\text{O.A.}}{U_{l,h}^2}\right)^{-0.19}$ $\frac{N_{\text{eff}}}{N} \leqslant 1$ $1.3(\text{s/m}) < \frac{U_g\text{O.A.}}{U_{l,h}^2} \leqslant 10^3(\text{s/m})$ $4.4\% < \text{O.A.} \leqslant 36\%$	$N = N_{\text{eff}}$, if O.A. < 5%, else N_{eff}/N decreases with increase in U_g and with decrease in U_l No significant effect of tray hole diameter Formation of gas cushion underneath the trays, which increases with U_g.
Kitai et al. (1969)	Co-current	$H_c = 130$ cm $D_c = 7$–14.5 cm 3 and 5 perforated trays $H_s = 10,\ 20$ cm O.A. = 2.4%–9.8% $d_0 = 0.2,\ 0.3,\ 0.5,\ 1$ cm $U_g = 1.83,\ 3.88,\ 4.15$ cm/s $U_l = 0.05$ cm/s	No correlations reported	Backmixing is a strong function of d_0. For $d_0 < 0.2$ cm, complete column sectionalization occurs For $d_0 > 0.2$ cm, only minor effect on liquid backmixing as U_g is increased. No effect of tray spacing.

stages interconnected in the direction of the main flow stream. Since all the tanks have the same volume, the mean residence time in each of them is equal to the mean residence time of the reactor system divided by the total number of mixed stages. It can be demonstrated that the total number of tanks in the model is equal to the inverse of the experimental dimensionless variance σ_D^2, which makes a straightforward model parameter estimation possible (Levenspiel, 1972). Table 2 summarizes the findings of published work, where the N-CSTR in series model was used to evaluate the experimental results. The ratio of the number of physical stages (number of trays plus one) to the number of effective stages (as calculated from the model) can be used to characterize the effect of different studied parameters on the liquid-phase mixing in trayed bubble columns. Blass and Cornelius (1997) used this approach to correlate the number of effective stages (N_{eff}) with the reactor operating conditions and the tray open area in a co-current trayed bubble column. They found that perfect agreement (e.g. number of effective stages equals the number of physical stages) always holds when the tray open area is less than 4.4% of the total tray cross sectional area for all the interval of superficial gas and liquid velocities tested. Moreover, when the tray open area was increased above 4.4% and up to 36%, then the authors observed that by increasing the superficial gas velocity and by reducing the superficial liquid velocity, the ratio of the number of effective stages to the number of physical stages decreased. It was postulated that the backmixing of liquid from stage to stage, and not an insufficient mixing within the stage, was responsible for this observation. The reason they offered to explain this phenomenon was that the formation of a cushion of gas underneath the trays sets a positive pressure gradient across the trays that causes liquid to drop back from the upper to the lower stage. However, if the superficial gas velocity is too high, then the upward momentum of gas will eventually stop the liquid backflow through the orifices. Nevertheless, they never experimentally verified this upper limit.

The N-CSTR in series model explains the liquid axial mixing in a very particular way. Since the tanks are perfectly mixed, there is intense short-range mixing that occurs when the liquid from one stage enters the next. However, no fraction of liquid that has moved to a position downstream of a given stage can ever come back. This is an unrealistic physical situation, especially when it is used to model trayed bubble columns with trays of large open areas and hole diameters, where inter-stage backmixing is expected. The model can be easily extended to account for liquid flowing from downstream locations by introducing liquid backflow streams into the conventional N-CSTR in series model configuration. Thus, in addition to the total number of stages N, a new model parameter, known as the backmixing coefficient k, is introduced. This parameter, which is defined as the ratio of the liquid backflow rate to the net liquid flow rate in the main direction of flow, can take values between zero (no liquid backflow) to infinite (total recirculation). Therefore, the model can describe the whole spectrum of axial mixing situations from plug flow ($N =$ infinite and $k = 0$) to total mixed flow ($k =$ infinite). Kats and Genin (1967) performed an extensive study of the liquid longitudinal mixing in a co-current sparged reactor sectionalized with sieve trays. The authors used the N-CSTR with backmixing model to interpret the results of their experiments, which were conducted in two trayed bubble columns of different heights and diameters, with a large number of different tray configurations (Table 3). Based on the velocity of the gas phase, the researchers distinguished four regions in which the nature of the longitudinal liquid mixing was found to be different. In the first region, $U_g = 0.01$ to 1 cm/s, the liquid mixing increases with gas velocity. It was

Table 3
Summary of surveyed published work where the N-CSTR with backmixing model is used to describe the liquid-phase mixing in trayed bubble columns

Reference	Gas–liquid arrangement	Apparatus and conditions	Correlation(s)	Main conclusions
Kats and Genin (1967)	Co-current	$H_c = 205,\ 600$ cm $D_c = 40,\ 95$ cm 4 and 9 perforated trays O.A. = 0.68%, 2.2%, 6%, 26.5% $d_0 = 0.15,\ 0.32,\ 0.8$ cm $\delta = 0.3$ cm $W_0 = 0.01$–100 cm/s $U_{l,h} = 0.022$–11 cm/s	Second region $k = 710^3 U_{l,h}^{-1.2} d_0^{2.12} \delta^{0.31} \left(\frac{H_c}{D_c}\right)^{-0.43}$ $U_{l,h} = \left(\frac{U_l}{3600\ \text{O.A.}}\right)$ Third region $k = 380 U_{l,h}^{-0.93} d_0 \delta^{0.64} H_c^{0.67} \log\left(\frac{\overline{W}_0}{W_0}\right)$ $\overline{W}_0 = 3.8\left(\frac{D_c}{d_0}\right)^{0.25}$ W_0 = superficial gas velocity in the holes of the trays W_0^T = superficial gas velocity in the holes of the trays, at which transition between regions 2 and 3 occurs	Backmixing increases with W_0 up to 1 m/s (first region) Absence of influence of gas velocity on the liquid backmixing up to a transitional gas velocity on the trays equal to W_0^T (second region) For $W_0 > W_0^T$, sharp reduction in the liquid backmixing with increasing gas velocity (third region) For $W_0 > 7$–13 m/s, absence of backmixing between stages $k = 0$ (fourth region)
Sekizawa and Kubota (1974)	Co-current	$H_c = 100, 120$ cm $D_c = 5, 10, 20$ cm 2,4,5 and 9 perforated trays $H_S = 10, 20, 40$ cm O.A. = 7% − 20.2% $d_0 = 0.2, 0.3, 0.5, 1, 1.5, 2$ cm $\delta = 0.3, 0.5, 1$ cm $U_g = 0.35$–9.25 cm/s $U_l = 0.12$–0.45 cm/s $\mu_l = 0.00913, 0.01, 0.0253,$ 0.0558, 0.0945, 0.165, 0.382 g/cm s $\sigma_l = 44.9, 66, 66.5, 67.1,$ 68.5, 68.7, 72.4 dyne/cm	$k = \frac{10.58\ U_g^{0.1}\text{O.A.}}{1 + 0.01(U_g/\text{O.A.})}\left(\frac{1}{U_l} - \frac{0.552}{U_l^{0.85}\text{O.A.}^{0.2}}\right) \Big/ \exp[(-1.5/d_0)(\mu_l^{0.5} + 0.01\delta^{0.2}/d_0)]$	For small tray O.A., k reaches maximum with an increase in U_g For large tray O.A., k increases monotonically with U_g Decrease in k with increase in U_l No liquid backflow across the trays for $d_0 < 0.2$ cm For 0.2 cm $< d_0 <$ 0.6 cm, sharp increase in k with increase d_0 For $d_0 > 0.6$ cm, small increase in k with increase in d_0 k is independent of D_c and H_S k decreases with increasing δ for $d_0 = 0.2$ cm, but is independent of δ for $d_0 > 0.2$ cm k decreases with increase in liquid viscosity μ_L k is independent of liquid surface tension σ_L

postulated that the diffusional nature of the mixing in this regime can explain the observations. The second region is characterized by the lack of effect of the gas velocity on the liquid axial mixing as the stages can be considered perfectly mixed. If the superficial gas velocity is further increased, a sharp reduction in the liquid mixing is observed (third region). Finally, when the gas velocity, as measured at the holes of the trays W_0, becomes larger than 13 m/s, the fourth region, which is characterized by a total absence of backflow between stages ($k = 0$), is reached.

Sekizawa and Kubota (1974) used the thermal tracer technique to study the effect of superficial gas and liquid velocities, column diameter, tray open area, tray hole diameter, tray spacing, tray thickness, liquid-phase viscosity and liquid-phase surface tension on the liquid-phase mixing in three different cocurrent trayed bubble columns for a wide range of experimental conditions (see Table 3). In the Thermal Tracer Technique, heat is supplied to the liquid, at constant rate, by a heater at the top of the column. Once the steady state is reached, the axial temperature profile is measured by thermocouples located along the column. By fitting the temperature profile to the solution of the steady state heat transfer equation, the backmixing coefficient k can be determined. In addition, Sekizawa and Kubota (1974) were able to correlate the backmixing coefficient with the variables studied and develop an empirical expression (Table 3).

3. Theory of tracer experiments

The analysis of the response of a system to a pulse input disturbance (i.e. injection of a tracer) is a commonly used technique for describing the mixing characteristics of chemical reactors (Levenspiel, 1972). Fig. 1 shows a schematic diagram of a reactor system in which a mass of a non-volatile tracer M_T is injected instantaneously at $t = 0$ into the reactor input stream. Here Q_L is the volumetric flow rate of the input stream. The transient tracer concentration response C_{out} is measured at the outlet of the reactor. The Exit Age Density Function of the system, also known as E-curve, can be obtained from the tracer response provided the following conditions are satisfied:

1. The time scale of the variations of the fluid flow pattern is orders of magnitude smaller than the tracer residence time in the reactor. We can assume that this is true in the steady state operation of the system.

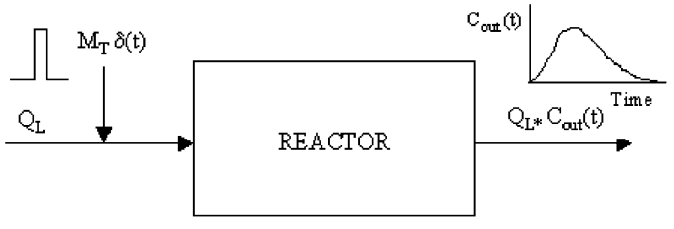

Fig. 1. Schematic diagram of a tracer pulse introduced into a reactor system and its response to the perturbation.

2. The tracer is confined in the tagged phase and no tracer is lost within the system by reaction or adsorption.
3. The tracer mixing cup concentration (flow averaged) is measured at the outlet of the reactor.
4. The boundaries of the system are "closed". This refers to the condition in which the flow at the inlet and outlet boundaries is dominated by convection and no molecule of tracer that has left the system can ever return back to it.

The tracer mass conservation equation around the system can be written as follows.

$$M_T = Q_L \int_0^\infty C_{\text{out}}(t)\,\mathrm{d}t. \tag{1}$$

If M_T and Q_L are known independently, then Eq. (1) can be used to assess the quality of the experimental technique used by checking the condition that the amount of tracer injected into the system has to be equal to the amount that leaves through the outlet.

The E-curve is equal to the normalized tracer concentration response. If there is a linear dependency between C_{out} and the response signal $R(t)$ measured in the experiments (e.g. conductivity signal of a conductive tracer), then $E(t)$ can be estimated as follows:

$$E(t) = \frac{C_{\text{out}}(t)}{\int_0^\infty C_{\text{out}}(t)\,\mathrm{d}t} = \frac{R(t)}{\int_0^\infty R(t)\,\mathrm{d}t} \tag{2}$$

$E(t)$ is a probability density function (PDF), therefore by definition, $E(t)\,\mathrm{d}t$ is equal to the fraction of the outflow that has resided in the system between time t and $t + \mathrm{d}t$. For a closed system, it can be demonstrated that the first moment of the E-curve is equal to the mean residence time of the tracer (Nauman and Buffham, 1983)

$$\mu_1 = \int_0^\infty t E(t)\,\mathrm{d}t = \bar{t}. \tag{3}$$

The second central moment $\mu_{2,c}$, also known as variance σ^2, measures the spread of the E-curve around the mean residence time.

$$\mu_{2,c} = \int_0^\infty (t-\mu_1)^2 E(t)\,\mathrm{d}t = \int_0^\infty t^2 E(t)\,\mathrm{d}t - (\bar{t})^2 = \sigma^2. \tag{4}$$

The mean residence time can be used to non-dimensionalize the E-curve. Then, a dimensionless exit age density function E^* and a dimensionless variance σ_D^2 can be written.

$$\theta = \frac{t}{\bar{t}}; \quad E^*(\theta) = E(t)\bar{t}, \tag{5}$$

$$\sigma_D^2 = \int_0^\infty E^*(\theta)\theta^2\,\mathrm{d}\theta - 1 = \frac{\sigma^2}{\bar{t}^2}. \tag{6}$$

The dimensionless variance measures the degree of internal backmixing in the reactor system. For non-pathological flows, σ_D^2 ranges between 0 (plug flow condition) and 1 (perfectly

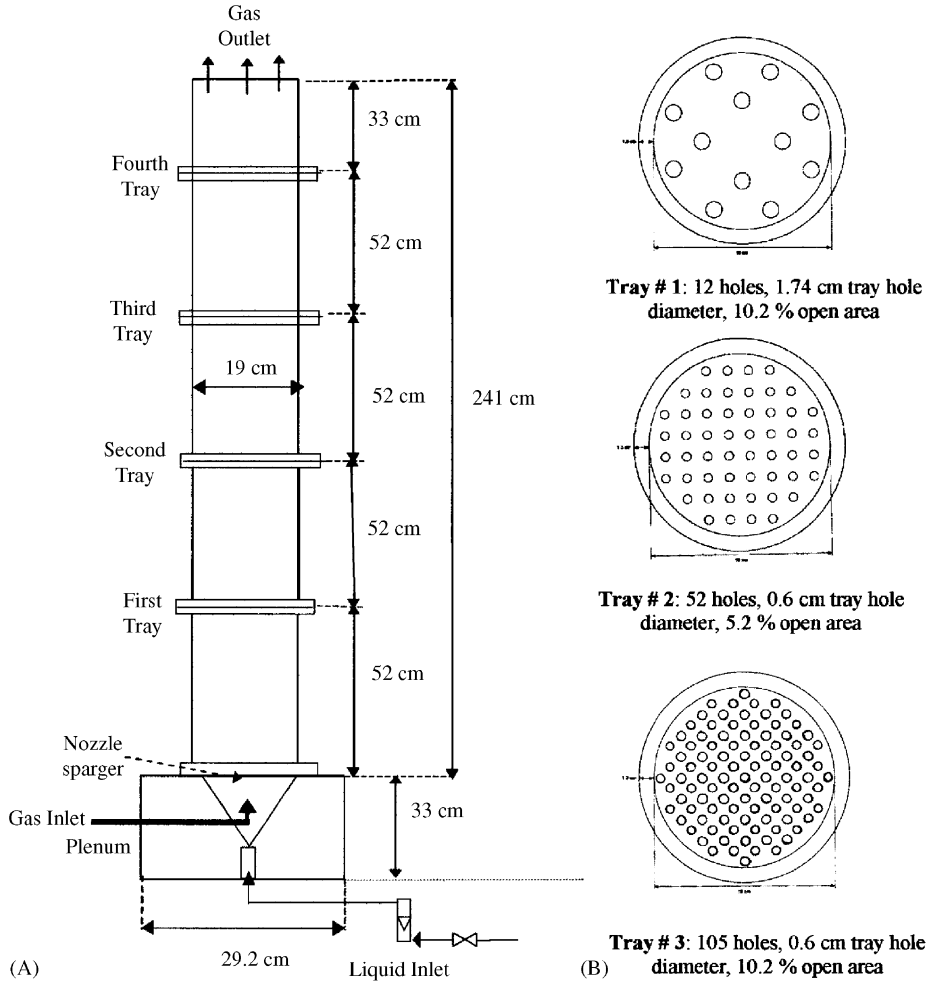

Fig. 2. (A). Schematic diagram of the trayed bubble column. (B) Geometric design and dimensions of the trays.

mixed condition). Pathological flows, such as bypass and stagnancy, are present in systems whose σ_D^2 is greater than 1.

The principle of convolution guarantees that if instead of an instantaneous injection of an amount of tracer M_T, the tracer perturbation at the inlet is equal to $C_{\text{in}}(t)$, then the output response signal $C_{\text{out}}(t)$ can be obtained from the convolution between $C_{\text{in}}(t)$ and the E-curve.

$$C_{\text{out}}(t) = \int_0^t E(t-\tau)C_{\text{in}}(\tau)\,\mathrm{d}t = E * C_{\text{in}}. \tag{7}$$

In practice, the evaluation of Eq. (7) from a discrete experimental input signal C_{in} is non-straightforward due to noise and round-off errors as reported by Mills and Dudukovic (1989). However, if care is taken in the experimental technique to make sure that the tracer injection time is orders of magnitude smaller than mean residence time of the tracer, then the assumption of instantaneous injection can be properly called. In this case, $C_{\text{in}}(t)$ can be assumed to be equal to the δ-Dirac function, and by substituting into Eq. (7) it can be proved that the E-curve is equal to $C_{\text{out}}(t)$.

$$C_{\text{out}}(t) = \int_0^t E(\tau)\delta(t-\tau)\,\mathrm{d}\tau = E(t). \tag{8}$$

Thus, by measuring the output response (e.g. tracer concentration) of a system to a pulse input perturbation (e.g. tracer injection), we can learn about the overall extent of internal backmixing in the system.

4. Experimental setup

A co-current trayed bubble column setup, which uses air and water as gas and liquid phases, respectively, has been constructed (Fig. 2). The column is made of four intermediate sections plus a top (disengagement) and a bottom (plenum) section, all built in plexiglas and attached together by flanges. The intermediate sections have an inside diameter of 19 cm and a total height of 52 cm each. The top section is 33 cm in height. There is also a 33 cm tall cone-shaped plenum section, where the gas and liquid phases enter the column and mix. The total height of the column from the base of the plenum to the top of the disengagement section is 241 cm. This is a five-stage unit with a total of four trays, which are mounted between the flanges. Three different types of trays were studied, whose design and geometric dimensions are shown in Fig. 2b. Tray types #1 and #3 both have the same total open area (10.2% O.A.),

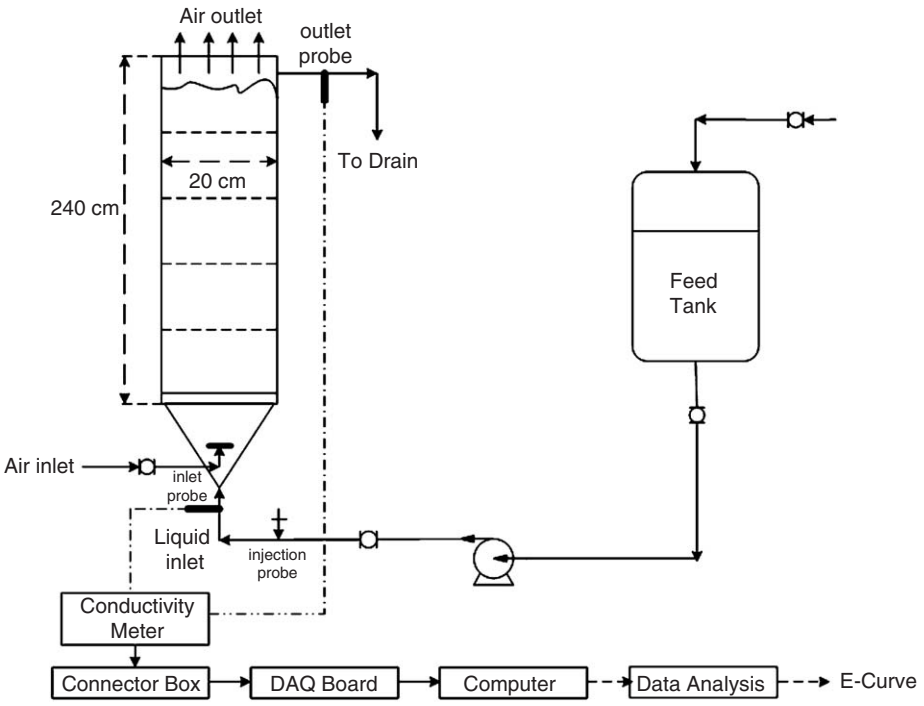

Fig. 3. Schematic diagram of the trayed bubble column with the tracer experimental setup.

but different hole diameters (1.74 cm and 0.6 cm, respectively). Conversely, tray types #2 and #3 share the same hole diameter (0.6 cm), but have different total open areas (5.2% and 10.2% O.A., respectively). A 9.5 mm in diameter single point nozzle, connected to a high pressure air line, is used to introduce compressed and filtered air through the bottom of the column. Water is pumped from a 750 l feed tank to the column, up to a maximum flow rate of 38 l/ min. Once the water fills the column, it overflows through the side of the column's upper section from where it is taken to the room sewer through a 5 cm diameter hose. Fig. 3 shows a schematic of the column along with the components of the setup used for the tracer experiments.

A pulse of a non-volatile liquid tracer, namely potassium chloride (KCl), is injected into the liquid feed stream at the bottom of the column. In water, KCl shows a wide region of linearity between the total amount of salt dissolved and the corresponding increase in the conductivity of the water. By trial and error, it was found that an injection of 10 cm^3 of a 0.2 g/cm^3 aqueous solution of KCl produces the best possible signal. The injection of the tracer was conducted with the help of a 10 cm^3 syringe, which had a 5 cm long and 17 gauge needle. The large diameter of the needle is necessary for a fast evacuation of the liquid tracer stored in the barrel of the syringe. The injection time was estimated to be less than one second. A conductivity probe (inlet conductivity probe) measures the conductivity of the liquid solution before it enters the column. The probe is mounted so that its tip remains always in the center of the 2.54 cm diameter PVC liquid feed pipe. The signal acquired by this probe serves as the base line signal used to assess the quality of the pulse injection. An external loop, fabricated in transparent PVC, was attached to the top section of the column at the gas–liquid disengagement plane. The purpose of this loop is to have a liquid mixing device, in which the liquid mixing cup concentration can be measured by a second conductivity probe (outlet conductivity probe). This probe was mounted at the base of the loop. The downstream end of the loop is connected to a plastic hose that takes the outlet liquid stream directly to the room sewer. The conductivity probes used in this work were obtained from Microelectrodes Inc. (MI-900 Series, dimensions: 0.635 cm in diameter by (30.5 cm long). They consist of two electrodes coated in black platinum, approximately 3 mm apart, and encased in plastic tubing. The probes were properly calibrated by measuring their response to solutions of different known tracer concentrations. The signals from the electrodes are transmitted to conductance meters (YSI Model 35), which provide a reading in units of conductance (ohm s^{-1}). In addition, the meters are interfaced to a PC through a Data Acquisition Board (AT-MIO-16E-10 from National Instruments Inc.). This configuration allows for a reliable on-line measurement and recording of the conductivity probes signals at a sampling frequency of 10 Hz. This value is three to four orders of magnitude larger than the characteristic frequency of the tracer wash-out curves at the experimental conditions covered in this work (10^{-3}–10^{-2} Hz). The above is needed to make sure that the changes in the conductivity of the liquid phase can be properly captured during the wash-out of the tracer in the column. It is well known that the continuous bubbling of gas over the tip of a conductivity probe causes the systematic lowering of the measured conductivity signal. Thus, when a bubble pierces the tip of the probe, a dip in the response signal is recorded since the electrical conductivity of air is orders ofmagnitude smaller than the liquid. As a result, in

addition to the response from the tracer injection, the raw signal measured by the outlet conductivity probe has a superimposed noise contribution coming from the bubble passage. Standard filtering schemes fail to properly "clean" the raw conductivity signal because they are based on the assumption that the noise has a randomly distributed variance with a zero time-average value. However, the noise introduced by the bubbles does not follow the previous assumptions, as it depends on the bubble dynamics inside the column. Gupta et al. (2000) proposed a robust filtering methodology that properly addresses the problem described above. The use of this methodology to filter the raw signals measured by the outlet conductivity probe in this work has turned out to be very successful (Alvaré, 2002).

The following range of superficial gas and liquid velocities was attempted in this study to cover both Bubbly and Churn-turbulent flow regimes in the bubble column with and without trays: $U_l = 0.5$, 1.0, and 1.5 cm/s; $U_g = 1$, 4, 8, 12, 16, and 20 cm/s. In addition, selective runs without gassing were executed as an exercise to study the effect of the absence of gas on the overall liquid phase mixing as compared to the case in gas–liquid conditions. However, several problems were encountered that made the collection of data at every single condition initially intended not viable. For instance, it was not possible to run the column simultaneously at $U_l = 1.5$ cm/s and high gas flow rates ($U_g > 12$ cm/s) due to the intense backpressure created by the mixing cup loop, which caused the column to flood.

5. Analysis of the experimental results

The injected pulse of KCl causes a sharp peak in the response signal of the inlet conductivity probe before it enters the column. For each of the runs, the time of the occurrence of the peak in the signal is considered to be the initial time ($t = 0$). In addition, the tracer injection time $\Delta t_{\text{injection}}$ can be approximately estimated from the width of the E-curve of the inlet conductivity probe. In order for the assumption of ideal pulse injection to be considered acceptable, Kastanec and Zahradnik (1973) recommended that the ratio of the injection time to the mean residence time of the tracer in the column $\bar{t}$ should be smaller than 0.05. As it turns out, this criterion is satisfied for all the experimental runs conducted in this work (Alvaré, 2002). Thus, according to Eq. (8), we can assume that the experimental E-curve is equal to the response signal of the outlet conductivity probe. The corresponding calibration curve of the outlet probe is used to convert the signal from its original units in Volts to concentration units in grams of KCl per cm^3. As an example, Fig. 4 shows the experimental E-curves at three different superficial liquid velocities, $U_l = 0.5$, 1.0, and 1.5 cm/s; and at $U_g = 8$ cm/s superficial gas velocity, obtained in the trayed bubble column with tray type #1 ($d_0 = 1.74$ cm, 10.2% O.A.).

The accuracy of the experimental method was checked by comparing the amount of tracer detected (Eq. (1)) with the total amount injected with the syringe into the column. In general, tracer mass conservation was satisfied with an average error of 10% and a maximum error of 15%.

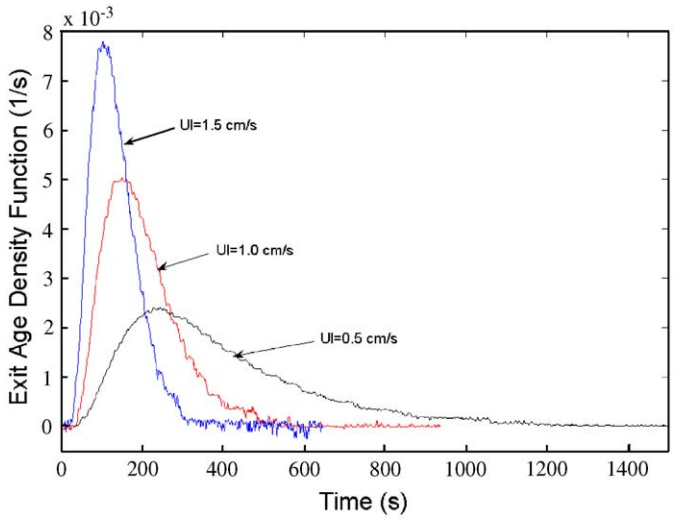

Fig. 4. Experimental E-curves obtained in the trayed bubble column with tray type #1 ($d_0 = 1.74$ cm, 10.2% O.A.) at $U_l = 0.5$, 1.0, and 1.5 cm/s and $U_g = 8$ cm/s.

The dimensionless variance σ_D^2 of the experimental E-curve (Eq. (6)) is shown versus superficial gas velocity in Fig. 5 for the bubble column with and without trays at $(A) U_l = 0.5$ cm/s and $(B) U_l = 1.5$ cm/s, respectively. The width of the error bars displayed in the plots covers a 95% confidence interval around the mean value. According to the results, it can be concluded that the placement of perforated trays in a conventional bubble column significantly reduces the overall liquid backmixing. In fact, for most of the experiments, more than a three-fold reduction in the variance of the experimental E-curves can be realized in the trayed bubble column as compared to the bubble column without trays. Moreover, only at the lowest superficial liquid velocity tested ($U_l = 0.5$ cm/s) the dimensionless variances in the column with tray type #1 ($d_0 = 1.74$ cm, O.A. = 10.2%) are statistically larger than the variances obtained with tray types #2 ($d_0 = 0.6$ cm, O.A. = 5.2%) and #3 ($d_0 = 0.6$ cm, O.A. = 10.2%). In fact, the effect of tray geometry is indistinguishable at $U_l = 1.5$ cm/s, as one can see in Fig. 5B.

Fig. 6 shows the dimensionless variances versus superficial gas velocity at three different superficial liquid velocities $U_l = 0.5$, 1.0, and 1.5 cm/s for the trayed bubble column with tray types #1 (A), #2 (B), #3 (C), and for the column without trays (D). It can be clearly observed that with an increase in the superficial liquid velocity, a decrease in the overall liquid backmixing follows. The decrease in the dimensionless variance is more important when the liquid velocity is incremented from $U_l = 0.5$ to 1.0 cm/s, than from $U_l = 1.0$ to 1.5 cm/s.

The liquid backmixing slightly increases with superficial gas velocity in the low value range of U_g, whereas it becomes almost independent of gas velocity at higher values. One hypothesis that could explain this observation is that in the range of low superficial gas velocities the stages are partially mixed. Then, as the gas velocity is increased, the growing degree of turbulence generated within the stages is responsible for the increase in liquid recirculation, which in turn enhances the

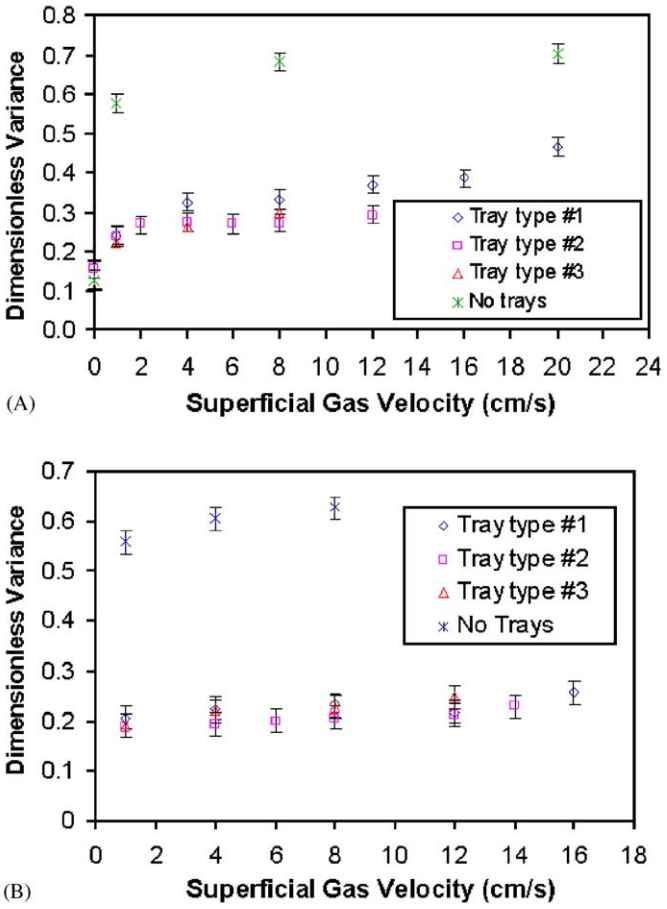

Fig. 5. Experimental dimensionless variance versus superficial gas velocity in bubble column with trays (tray types #1, #2, and #3) and without trays at superficial liquid velocities (A) $U_l = 0.5\,\mathrm{cm/s}$ and (B) $U_l = 1.5\,\mathrm{cm/s}$.

interstage backmixing. However, after a certain gas velocity, the stages become perfectly mixed and the increasing upward momentum of the gas and the liquid eventually prevent the liquid backmixing between stages. As a result, further increases in U_g have little or no effect on the overall liquid mixing.

The flow of gas is responsible for the characteristic liquid circulation pattern in the column and thereby for the intense liquid backmixing as compared to single phase flow. This can be seen, for instance, in Figs. 7B and D, where the variance of the experimental E-curves obtained in single phase flow conditions (no gassing) is significantly smaller than in gas–liquid conditions, even when compared to the smallest superficial gas velocity tested ($U_g = 1\,\mathrm{cm/s}$).

In general, these results agree with the findings of Palaskar et al. (2000). The authors pointed out that with a reduction in the tray open area and/or the diameter of the holes, there is an associated increase in the resistance of the gas flow across the trays. This flow resistance enhances the gas distribution in the radial direction in each of the stages, which in turn reduces the liquid recirculation velocity and therefore results in a lower overall liquid backmixing. Similarly, the interstage backmixing is lowered with a reduction in tray open area and tray hole diameter.

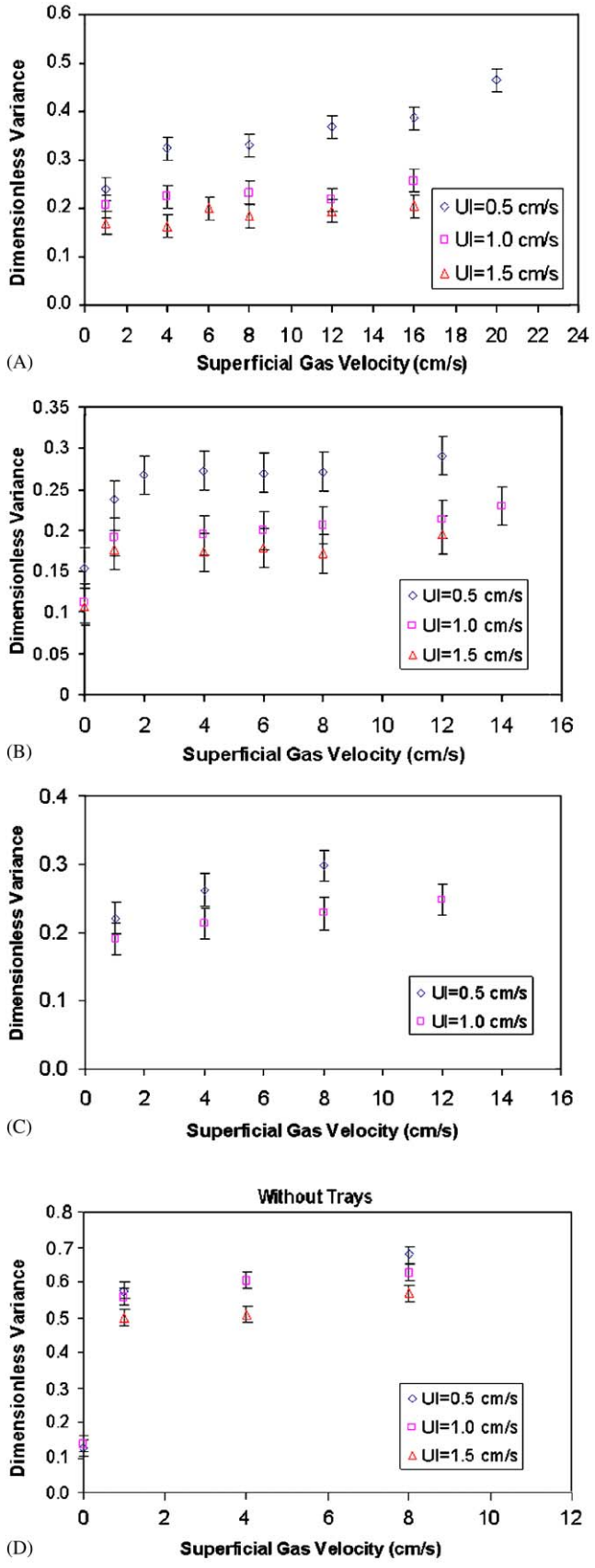

Fig. 6. Experimental dimensionless variance versus superficial gas velocity in trayed bubble column with tray types #1 (A), #2 (B), #3 (C), and in bubble column without trays (D) at superficial liquid velocities $U_l = 0.5$, 1.0, and 1.5 cm/s.

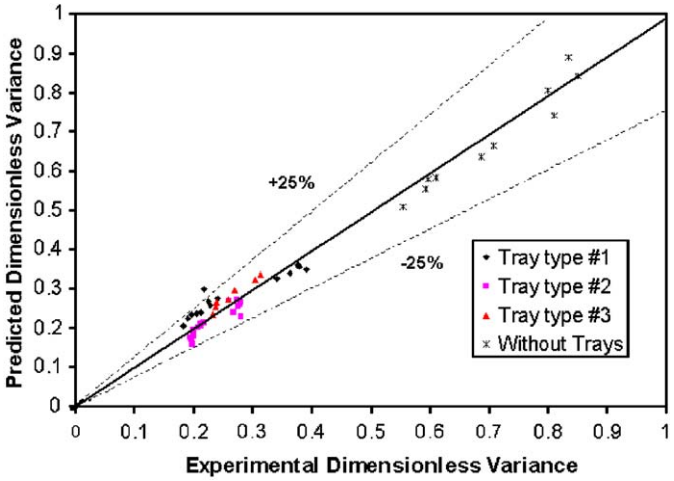

Fig. 7. Comparison of the dimensionless variance of the E-curve between the tracer experiments and the predictions of Eq. (9).

The available experimental data can be used to correlate the dimensionless variance of the E-curve (σ_D^2) with the studied variables. Thus, the variance can be written as a power function of the superficial liquid velocity (U_g), the superficial gas velocity (U_l), the tray hole diameter to column diameter ratio (d_0/D_c), and the tray open area (O.A.) (Eq. (9)).

$$\sigma_D^2 = C U_l^a U_g^b \left(\frac{d_0}{D_c}\right)^c \text{O.A.}^d. \tag{9}$$

Multivariable linear regression analysis has been conducted to determine the value of the coefficients C, a, b, c, and d that provides the best fit for σ_D^2. The value of the exponents in Eq. (9), along with their 95% confidence intervals, is the following: $C = 0.585$, $a = -0.341 \pm 0.080$, $b = 0.062 \pm 0.037$, $c = 0.011 \pm 0.109$, $d = 0.384 \pm 0.133$.

A total of 49 data points, each corresponding to a different set of experimental conditions, were used to fit the parameters in Eq. (9). The range of the values for the different variables studied is as follows: $U_l = 0.5$–1.5 cm/s, $U_g = 1$–18 cm/s, $d_0/D_c = 0.0315$–1, and O.A. $= 0.052$–1.

The comparison between the experimental data points and the predictions of Eq. (9), is shown in the corresponding Parity Plot (Fig. 7). The figure shows that the values predicted by Eq. (9) are within ±25% of the experimental dimensionless variances. The mean relative error between experimental data and predictions is 9%.

6. Model interpretation of the experimental results

As already stated in the literature review, a good strategy to choose the proper liquid mixing model should be based upon the agreement of the physical model conception with the real reactor arrangement. In addition, a good model should offer a balance between an accurate physical realization of the real system with the minimum number of parameters for a straightforward and univocal interpretation of the experimental data.

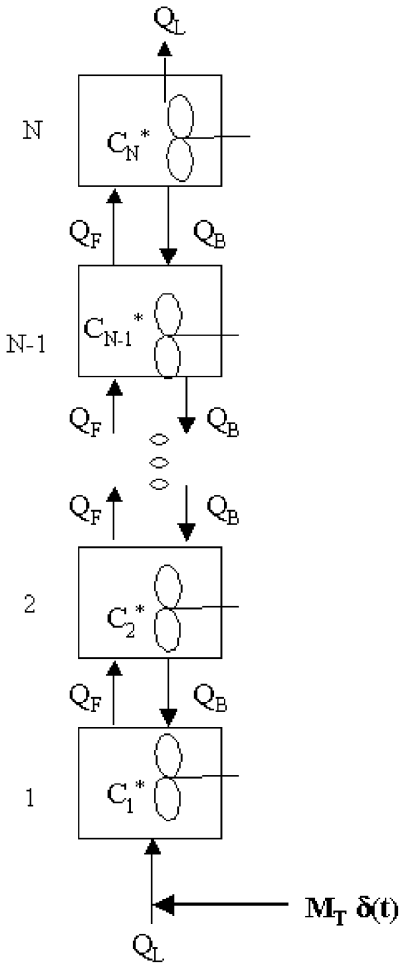

Fig. 8. Schematic diagram of the N-CSTR with backmixing model.

The model parameters are determined by finding the best fit of the model to the experimental data.

The N-CSTR with Backmixing Model and the ADM have been selected as the models of choice to describe the experimental overall liquid mixing in the co-current trayed bubble column. Further, the predictions of the two models will be compared.

7. The N-CSTR with backmixing model

The N-CSTR with backmixing model can be used to describe the time evolution of a given amount M_T of a tracer species, which is injected as an ideal pulse, at time zero, into the liquid inlet stream in the first tank of the series (Fig. 8). The perfectly mixed model assumption assures that the injected tracer gets instantaneously and homogenously mixed into the first stage of the series. By writing the transient tracer mass conservation equations in each of the perfectly mixed stages, the following set of ordinary differential equations can be written.

$$\frac{dC_1^*}{d\theta} = kC_2^* - (1+k)C_1^*, \quad \text{First stage, } i = 1, \tag{10}$$

$$\frac{dC_i^*}{d\theta} = (1+k)C_{i-1}^* - (1+2k)C_i^* + kC_{i+1}^*,$$

Intermediate stage, $i = 2$ to $N-1$, (11)

$$\frac{dC_N^*}{d\theta} = (1+k)C_{N-1}^* - (1+k)C_N^*, \quad \text{Last stage, } i = N. \quad (12)$$

The above set of ordinary differential equations need to be solved along with the following initial conditions:

$$C_1^*(\theta=0) = N, \quad C_2^*(\theta=0) = C_3^*(\theta=0) = \cdots = C_i^*(\theta=0) = \cdots = C_N^*(\theta=0) = 0 \quad (13)$$

C_i^* and θ_i, which are the dimensionless tracer concentration in the ith tank and the dimensionless time, are defined below.

$$C_i^* = \frac{C_i}{C_T} = \frac{C_i}{M_T/[V_i N(1-\bar{\varepsilon}_g)]}, \quad (14)$$

$$\theta = \frac{t}{\bar{t}} = \frac{t}{[V_i N(1-\bar{\varepsilon}_g)/Q_L]} \quad (15)$$

C_i is the liquid-phase tracer concentration in the ith tank of the series, $\bar{C}_T$ is the liquid-phase average tracer concentration, $\bar{t}$ is the tracer residence time, and $\bar{\varepsilon}_g$ is the overall gas holdup in the system. The overall gas holdups in the column, with and without trays, have been experimentally measured and documented by Alvaré (2002).

The number of well mixed tanks or stages N can take integer values between 2 and infinity (plug flow model). The backmixing coefficient k is defined as the ratio of the liquid backflow rate Q_B to the net liquid flow rate Q_L.

$$k = \frac{Q_B}{Q_F - Q_B} = \frac{Q_B}{Q_L}. \quad (16)$$

Therefore, the versatility of the model makes it possible to describe the whole spectrum of mixing situations from plug flow (N = infinite and $k = 0$) to total mixed flow (k = infinite).

Eqs. (10)–(12) along with the corresponding initial conditions (Eq. (13)) form a simple linear eigenvalue problem, which can be solved by matrix inversion or by a Runge–Kutta algorithm scheme. The solution of the equations gives the dimensionless transient concentrations of the tracer in each of the stages ($C_1^*, C_2^*, \ldots, C_{N-1}^*, C_N^*$). It can be easily demonstrated that the dimensionless model exit age density function E_M^* is equal to the dimensionless tracer concentration in the last stage of the series C_N^* (Nauman and Buffham, 1983).

In order to determine the model parameters N and k, a time domain fitting scheme has been implemented based on the minimization of the objective function $R^t(N,k)$ (Eq. (17)).

$$R^t(N,k) = \sqrt{\sum_{j=1}^{t_{\text{total}}} \left[\frac{E_E^*(\theta_j) - E_M^*(\theta_j, N, k)}{t_{\text{total}} - 2}\right]^2}$$

$$j = 1, \ldots, t_{\text{total}}. \quad (17)$$

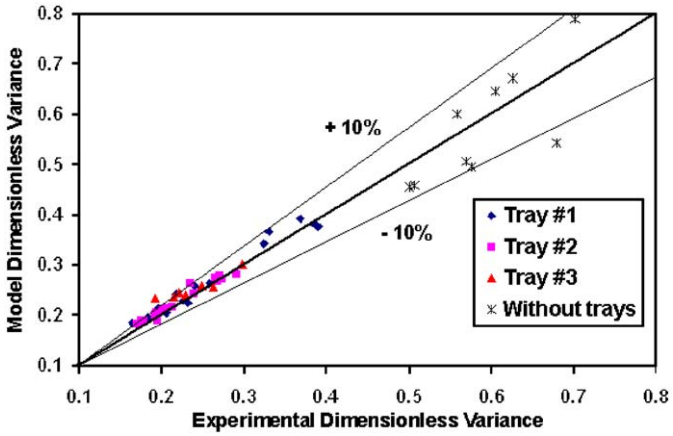

Fig. 9. Comparison between the experimental and the model-predicted (N-CSTR with backmixing model) dimensionless variances.

Here, $E_E^*(\theta_j)$ and $E_M^*(\theta_j, N, k)$ are the experimental and the model dimensionless exit age density functions evaluated at the jth time data point θ_j, and t_{total} is equal to the total number of time data points available for each run. A least squares minimization routine was written and executed in MATLAB™ (The MathWorks Inc.), the details of which have been reported by Alvaré (2002). This fitting procedure is repeated for each available experimental run to obtain the values of N, and k that better match the corresponding experimental exit age density function (E-curve). The total number of stages N found varied between 3 and 7 (integer values only), whereas the backmixing coefficient k varied between 0 and 2.

Roemer and Durbin (1967) transformed Eqs. (10)–(13) into the Laplace domain and using the Method of the Moments, they derived the exact analytical expression for the dimensionless variance of the tracer in the last stage (Eq. (18)).

$$\sigma_D^2 = \frac{1+2k}{N} - \frac{2k(1+k)\left(1 - \left(\frac{k}{1+k}\right)^N\right)}{N^2}. \quad (18)$$

Fig. 9 shows the comparison between the experimental and the model dimensionless variances. The model-predicted values were calculated by substituting the corresponding fitted values of the parameters N and k into Eq. (18). It can be seen that most of the predicted model variances are within ±10% of their corresponding experimental values.

8. The axial dispersion model (ADM)

In a non-reactive gas-liquid system, the transient ADM equations for an ideal pulse injection $\delta(\theta)$ (Dirac Delta function) of a non-volatile liquid tracer species at the reactor inlet with closed-closed boundary conditions can be written as follows (Myers, 1986).

$$\frac{\partial C^*(Z,\theta)}{\partial \theta} = -\frac{\partial C^*(Z,\theta)}{\partial Z} + \frac{1}{Pe}\frac{\partial^2 C^*(Z,\theta)}{\partial Z^2}, \quad (19)$$

$$-\frac{1}{Pe}\frac{\partial C^*(Z,\theta)}{\partial Z}+C^*(Z,\theta)=\delta(\theta)\quad \text{at } Z=0;$$

$$\delta(\theta)=\left\{\begin{matrix}\infty & \text{at } \theta=0\\ 0 & \text{at } \theta\neq 0\end{matrix}\right\}, \tag{20}$$

$$\frac{\partial C^*(Z,\theta)}{\partial Z}=0\quad \text{at } Z=1, \tag{21}$$

$$C^*(Z,\theta)=\delta(Z)\quad \text{at } \theta=0;\quad \delta(Z)=\left\{\begin{matrix}\infty & \text{at } Z=0\\ 0 & \text{at } Z\neq 0\end{matrix}\right\} \tag{22}$$

C^*, Z, and θ are the dimensionless liquid-phase tracer concentration, the dimensionless axial coordinate, and the dimensionless time, respectively. These are defined below.

$$C^*=\frac{C}{\bar{C}_T},\quad Z=\frac{z}{L},\quad \theta=\frac{tU_l}{(1-\bar{\varepsilon}_g)L}. \tag{23}$$

The Peclet number is the only parameter of the ADM and it can be mathematically defined as follows.

$$Pe=\frac{U_l L}{D_L(1-\bar{\varepsilon}_g)}. \tag{24}$$

Brenner (1962) used the Method of Eigenfunction Expansions to solve Eq. (19) with closed-closed boundary conditions (Eqs. (20) and (21)) and initial condition (Eq. (22)). He found the following series solution (Eq. (25)) for the transient tracer concentration at the outlet of the system ($Z=1$).

$$C^*(1,\theta)=E_M^*(\theta)=e^{Pe/2}\sum_{n=0}^{\infty}\left[\frac{2w_n\sin(w_n)[Pe^2+4w_n^2]\exp\left[-\dfrac{Pe^2+4w_n^2\theta}{4Pe}\right]}{Pe[Pe^2+4w_n^2+4Pe]}\right]. \tag{25}$$

Here, w_n are the positive roots of the following expression:

$$\tan(w_n)=\frac{4w_nPe}{4w_n^2-Pe^2}. \tag{26}$$

The series converges very slowly for small times and hence it is not very convenient to be used for fitting purposes. However, the Laplace domain fitting is more appropriate since the model transfer function (Eq. (27)) can be obtained from the solution of Eqs. (19)–(22) in the Laplace domain (Nauman and Buffham, 1983).

$$C^*(1,s^*)=E_M^*(s^*)=\frac{4a(s^*)\exp\left[\dfrac{Pe}{2}(1-a(s^*))\right]}{(1+a(s^*))^2-(1-a(s^*))^2\exp[-Pe\,a(s^*)]}, \tag{27}$$

$$a(s^*)=\sqrt{1+\frac{4s^*}{Pe}}. \tag{28}$$

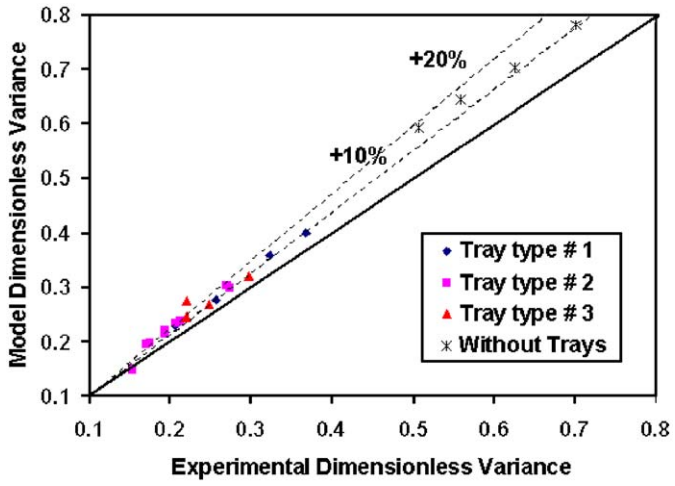

Fig. 10. Comparison between the experimental and the model-predicted (Axial Dispersion Model) dimensionless variances.

Applying the method of the moments (Nauman and Buffham, 1983) to the model transfer function (Eq. (27)), the second moment or dimensionless variance around the mean residence time at the outlet boundary of the system can be easily derived.

$$\sigma_D^2=\frac{2}{Pe}-\frac{2}{Pe^2}(1-e^{-Pe}). \tag{29}$$

A fitting algorithm was implemented to estimate the model parameter (Peclet number) from the experimental results in the Laplace domain (Alvaré, 2002). This procedure minimizes the objective function $R^L(Pe)$ (Eq. (30)).

$$R^L(Pe)=\sqrt{\sum_{j=1}^{t_{\text{total}}}\frac{[E_E^*(s_j^*)-E_M^*(s_j^*,Pe)]^2}{t_{\text{total}}-1}}\qquad j=1,\ldots,t_{\text{total}}. \tag{30}$$

Here, $E_E^*(s_j^*)$ and $E_M^*(s_j^*)$ are the Laplace-domain experimental and model dimensionless Exit Age Density functions evaluated at the jth Laplace-domain data point s_j^*, and t_{total} is the total number of Laplace-domain data points available. $E_E^*(s^*)$ is obtained by applying the Laplace Transformation (Eq. (31)) to the experimental dimensionless time-domain E-curve $E_E^*(\theta_i)$.

$$E_E^*(s_j^*)=\sum_{i=0}^{t_{\text{total}}}E_E^*(\theta_i)\exp(-s_j^*\theta_i)\Delta\theta_i. \tag{31}$$

The fitted Peclet numbers varied between 2.3 and 12.7. Fig. 10 shows the comparison of the experimental and the model dimensionless variances. The latter are calculated by substituting the fitted values of Peclet number into Eq. (29). As it can be seen, the model overpredicts the experimental variances from +10% to +20%.

For a given Pe number, the time-domain dimensionless ADM E-curve, $E_M^*(\theta,Pe)$, can be obtained by numerically inverting the corresponding Laplace-domain transfer function $E_M^*(s^*,Pe)$ (Eq. (27)). The numerical inversion algorithm described by De Hoog et al. (1982) was used for this purpose.

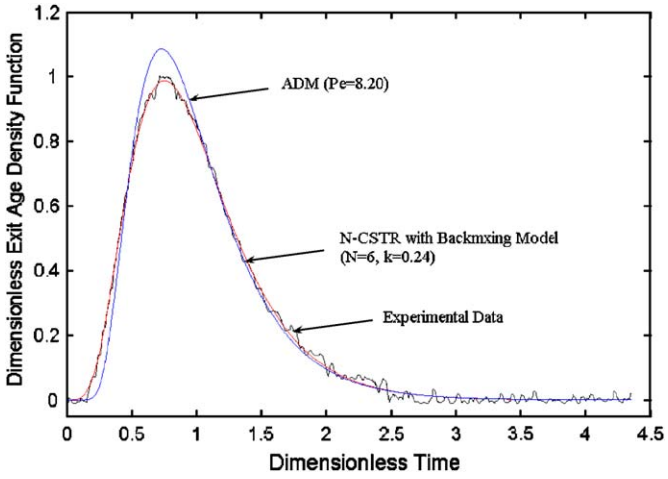

Fig. 11. Comparison of the experimental E-curves versus the ADM (Pe=8.20) and the N-CSTR with backmixing model ($N=6$, $k=0.24$) E-curves obtained in the trayed bubble column with tray type #1 ($d_0 = 1.74$ cm, 10.2% O.A.) at $U_l = 1$ cm/s and $U_g = 4$ cm/s.

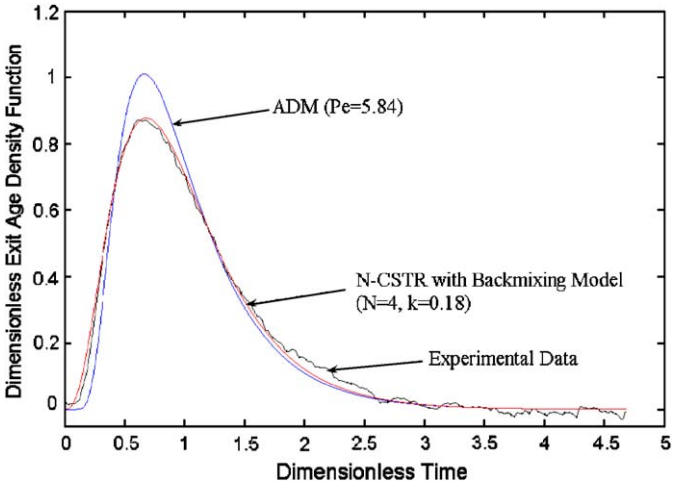

Fig. 13. Comparison of the experimental E-curves versus the ADM (Pe=5.84) and the N-CSTR with backmixing model ($N=4$, $k=0.18$) E-curves obtained in the trayed bubble column with tray type #3 ($d_0 = 0.6$ cm, 10.2% O.A.) at $U_l = 0.5$ cm/s and $U_g = 8$ cm/s.

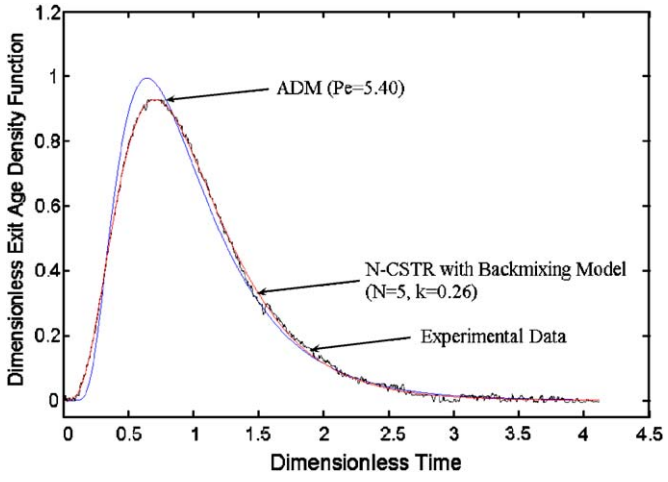

Fig. 12. Comparison of the experimental E-curves versus the ADM (Pe=5.40) and the N-CSTR with backmixing model ($N=5$, $k=0.26$) E-curves obtained in the trayed bubble column with tray type #2 ($d_0 = 0.6$ cm, 5.2% O.A.) at $U_l = 0.5$ cm/s and $U_g = 8$ cm/s.

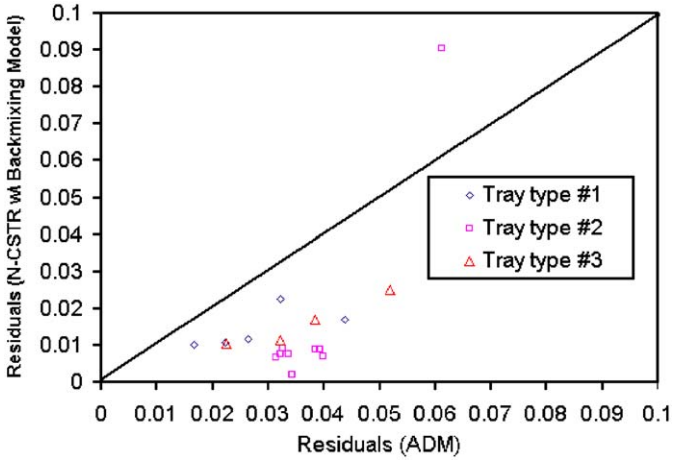

Fig. 14. Comparison of the residuals of the fit of the experimental tracer E-curves between the N-CSTR with backmixing model $R^T(N,k)$ and the ADM $R^T(Pe)$.

9. Comparison between the predictions of the models

As an example of the comparison between the predictions of the two models, Figs. 11–13 show the experimental and the corresponding fitted model E-curves at selected conditions for tray types #1 ($d_0 = 1.74$ cm, O.A. = 10.2%), #2 ($d_0 = 0.6$ cm, O.A. = 5.2%), and #3 ($d_0 = 0.6$ cm, O.A. = 10.2%), respectively. The ADM seems to always over predict the maximum of the experimental E-curves, whereas the N-CSTR with backmixing model follows the curves through the entire domain. A similar trend was observed for most of the experimental conditions covered in this study.

The comparison between the residuals of the fits for the two models can help to quantitatively verify whether one of the models is able to explain the experimental data better than the other over the entire time domain of the E-curve for all range of the experimental conditions covered in this work. Fig. 14 shows the residuals of fit given by the N-CSTR with backmixing model $R^t(N,k)$ (Eq. (17)) versus the residuals given by the ADM $R^t(Pe)$ (Eq. (32)).

$$R^t(Pe) = \sqrt{\sum_{i=1}^{t_{\text{total}}} \frac{[E_E^*(\theta_i) - E_M^*(\theta_i, Pe)]^2}{t_{\text{total}} - 1}} \quad i = 1, \ldots, t_{\text{total}}. \tag{32}$$

Each of the points in Fig. 14 corresponds to the residuals of the fits given by the two models for a given set of experimental conditions (U_l, U_g, and type of tray). As it can be observed,

most of the points are located below the diagonal line in the plot, which indicates that the residuals of the fit yielded by the ADM seem to be larger than the residuals of the N-CSTR with backmixing model. A statistical analysis (two-sample t-test) has been conducted to confirm whether the above observation can be statistically supported or not. The two-sample t-test is used to determine if the means of two normally distributed populations are equal (Box et al., 1979). In this case, the two populations are the residuals of the fits given by the two models $R^t(N_i, k_i)$ and $R^t(Pe_i)$. Assuming that the differences of the residuals of the fits $d = R^t(N, k) - R^t(Pe)$ form a normally distributed population with mean δ and variance σ^2. The method tests if δ is equal to zero, in which case it would prove that $R^t(N, k)$ and $R^t(Pe)$ are part of the same population.

The values of δ and σ^2 are not known since only a small sample of data points (n) of the larger population is available to us. Further, it can be demonstrated (Box et al., 1979) that if $\bar{d}$ and S_d are, respectively, the mean (Eq. (33)) and the standard error (Eq. (34)) of this smaller sample, then t (Eq. (35)) follows a t-distribution with $n - 1$ degrees of freedom and with a standard error of the mean equal to $S_{\bar{d}}$ (Eq. (36)).

$$\bar{d} = \frac{\sum_{i=1}^{n} d_i}{n}, \tag{33}$$

$$S_d = \sqrt{\frac{\sum_{i=1}^{n} (d_i - \bar{d})^2}{n-1}}, \tag{34}$$

$$t = (\bar{d} - \delta)/S_{\bar{d}}, \tag{35}$$

$$S_{\bar{d}} = S_d/\sqrt{n}. \tag{36}$$

The probability that the real mean of the differences of the residuals (δ) is equal to zero (Null Hypothesis) can be put to test since the probabilities of the t-distribution for $n - 1$ degrees of freedom are available (Box et al., 1979). Hence if the probability that t is equal to $(\bar{d}-0)/S_d/\sqrt{n})$ is equal or smaller than 5%, then the Null Hypothesis ($\delta=0$) can be statistically rejected. In other words, δ is different than zero and the residuals given by the two models can be said to be statistically different. Otherwise, if the Null Hypothesis cannot be rejected, then it can be stated, with a probability equal to or greater than 95%, that the efficacy of the N-CSTR with backmixing model and the ADM to fit the experimental tracer data cannot be differentiated.

Substituting into Eqs. (33) to (36), the following results can be estimated from a sample of $n = 18$ data points: $\bar{d} = -0.019$, $S_d = 0.015$, $S_{\bar{d}} = 3.53 \times 10^{-3}$, and $t = -5.672$.

Looking at the tables for a t-distribution with $n - 1 = 17$ degrees of freedom, then the probability that t is equal to or smaller than -5.672 is equal to 0.001%, which is much smaller than the 5% significance level. Hence, the Null Hypothesis can be very comfortably rejected. In summary, it has been statistically demonstrated that the residuals of the fit yielded by the N-CSTR with backmixing model are significantly smaller than the residuals obtained by the ADM and, therefore, the former model fits the experimental tracer E-curves better than the latter model.

As a rule of thumb, the ADM should be used with caution for Peclet numbers smaller than 20 (Dudukovic and Felder, 1983). This relates to the fact that the ADM fails to provide good predictions for large deviations from plug flow behavior. The Peclet numbers estimated in this work ranged from 1, in the case of the column without trays, to a maximum of 9, in the case of the trayed bubble column with tray type #2 at $U_l = 1.5$ cm/s and $U_g = 1$ cm/s.

Therefore, the results suggest that a stagewise model such as the N-CSTR with backmixing model seems better suited to describe the overall liquid-phase backmixing in trayed bubble column reactors than the ADM.

10. Summary and conclusions

An experimental bench-scale Trayed Bubble Column has been constructed to study the effect of the trays and the flow operating conditions (superficial gas and liquid velocities) on the overall liquid-phase mixing. The interpretation of liquid-phase tracer response experiments, conducted in the column with three different types of trays at a range of superficial gas and liquid velocities, was used to quantify the extent of liquid backmixing in the column. It has been found that the placement of perforated trays inside conventional bubble columns drastically reduces the overall liquid mixing by decreasing the liquid circulation velocity inside the stages and by restricting the backmixing of liquid between stages. Trays of smaller open areas and smaller hole diameters offer more resistance to the gas–liquid flow in the column, which in turn helps to further reduce the liquid backmixing. This study has shown that tray open area has a stronger effect on the extent of liquid backmixing reduction than tray hole diameter. An increase in the superficial liquid velocity results in the reduction of the liquid backmixing in the column when the gas and liquid phases are operated co-currently in the upward direction. In addition, liquid mixing slightly increases with superficial gas velocity in the low value range of U_g, whereas it becomes almost independent of gas velocity at higher values. Moreover, an empirical expression that correlates the variance of the dimensionless tracer E-curve with all the variables studied (tray open area, tray hole diameter, and superficial gas and liquid velocities) has been developed.

The Axial Dispersion Model (ADM) and the N-CSTR with Backmixing Model were used to fit the experimental exit age density function curves (E-curves), obtained from the tracer tests, to the model E-curves. It was statistically proved that the N-CSTR with Backmixing Model matches the experimental E-curves significantly better than the ADM. This result supports the hypothesis that a stagewise model, such as the N-CSTR with Backmixing Model, offers a more realistic representation of the liquid mixing phenomena in a trayed bubble column than the ADM.

Notation

C	tracer concentration, g/L
C_T	average tracer concentration, g/L
C^*	dimensionless tracer concentration
$\bar{d}$	mean value of the differences between the residuals of the fits (Eq. (33))
d_0	tray hole diameter, cm
D_c	column diameter, cm
D_L	liquid-phase axial dispersion coefficient, $cm^2\,s^{-1}$
$E(t)$	Exit Age Density Function or E-curve, s^{-1}
$E^*(\theta)$	dimensionless Exit Age Density Function or dimensionless E-curve
$E(s)$	Laplace-transform of $E(t)$
$E^*(s^*)$	Laplace-transform of $E^*(\theta)$
g	acceleration due to gravity, $9.81\,m\,s^{-2}$
H_c	height of the column, cm
H_S	height of the stage or tray spacing, cm
k	backmixing coefficient
L	length scale, cm
M_T	mass of tracer, g
n	number of data points
N	number of stages or number of tanks
N_{eff}	number of effective stages
O.A.	open area of the tray
Pe	Peclet number (Eq. (24))
Q_B	backward liquid flowrate, $cm^3\,s^{-1}$
Q_F	forward liquid flowrate, $cm^3\,s^{-1}$
Q_L	net liquid flowrate, $cm^3\,s^{-1}$
$R(t)$	tracer response signal, g/L
R^t	residual of the fit function
R^L	Laplace transform function of R^t
s	Laplace-transform variable
s^*	dimensionless Laplace-transform variable
S_d	standard error of the differences between the residuals of the fits (Eq. (34))
$S_{\bar{d}}$	standard error of the mean of the differences between the residuals of the fits (Eq. (36))
t	time, s
$\bar{t}$	mean residence time, s
t_{total}	total number of experimental time data points
U_g	superficial gas velocity, $cm\,s^{-1}$
V	volume, cm^3
V_S	gas–liquid slip velocity, $cm\,s^{-1}$
W_0	superficial gas velocity in the holes of the tray, $cm\,s^{-1}$
z	axial location, cm
Z	dimensionless axial location

Greek letters

δ	thickness of the trays, cm
$\delta(\theta)$	Dirac Delta function
Δt_{tracer}	tracer injection time, s
$\bar{\varepsilon}_g$	overall gas holdup
θ	dimensionless time
μ_1	first moment of the E-curve, s
$\mu_{2,c}$	second central moment of the E-curve, s^2
μ_l	viscosity of the liquid phase, $g\,cm^{-1}\,s^{-1}$
ρ_g	density of the gas phase, $g\,cm^{-3}$
ρ_l	density of the liquid phase, $g\,cm^{-3}$
σ_1	viscosity of the liquid phase (dyne cm^{-1})
σ^2	variance, s^2
σ_D^2	dimensionlessvariance

Subscripts

ADM	Axial Dispersion Model
B	backward
c	column
eff	effective
E	experimental
F	forward
G, g	gas
h	hole
i	ith component
in	inlet
L, l	liquid
M	model
out	outlet
S	stage
t	time
T	tracer

Superscripts

$*$	dimensionless variable
L	Laplace-domain
t	time-domain

Acknowledgements

The industrial sponsors of the Chemical Reaction Engineering Laboratory (CREL) are gratefully acknowledged for providing the financial support required for this research work.

References

Alvaré, J., 2002. Gas holdup and liquid phase mixing in trayed bubble column reactors. M.S. Thesis, Department of Chemical Engineering, Washington University, St. Louis, U.S.A.

Blass, E., Cornelius, W., 1997. The residence time distribution of solid and liquid in multistage bubble columns in the co-current flow of gas, liquid, and suspended solids. Multiphase Flow 3, 459–469.

Box, G.E.P., Hunter, W.G., Hunter, J.S., 1979. Statistics for Experimenters. Wiley Series in Probability and Mathematical Statistics. Wiley, New York.

Brenner, H., 1962. Diffusion model of longitudinal mixing in beds of finite length-numerical values. Chemical Engineering Science 17, 229–243.

Chen, B.H., Yang, N.S., 1989. Characteristics of a co-current multistage bubble column. Industrial Engineering Chemistry Research 28, 1405–1410.

De Hoog, F.R., Knight, J.H., Stokes, A.N., 1982. An improved method for numerical inversion of Laplace transforms. S.I.A.M. Journal on Scientific Computing 3, 357–366.

Dreher, A.J., Krishna, R., 2001. Liquid phase backmixing in bubble columns, structured by introduction of partition plates. Catalysis Today 69, 165–170.

Dudukovic, M.P., Felder, R.M., 1983. Mixing Effects in Chemical Reactors-III–Dispersion Model. A.I.Ch.E Modular Instruction Series, Series E, vol. 4(6). American Institute of Chemical Engineers.

Dudukovic, M.P., Chen, J.C., Fan, L.S., Degaleesan, S., Gupta, P., Al-Dahhan, M.H., Toseland, A.B., 1999. Fluid dynamic parameters in bubble columns with internals. Chemical Engineering Science 54, 2187–2197.

Gupta, P., Al-Dahhan, M.H., Dudukovic, M.P., Mills, P., 2000. A novel signal filtering methodology for obtaining liquid phase tracer responses from conductivity probes. Flow Measurement Instrumentation 11 (2), 123–131.

Ichikawa, Y., Akachi, Y., Makino, K., 1967. On the Longitudinal Mixing Characteristics of Gas Bubble Column with Perforated Plates. Kagaku kogaku, abridged ed., pp. 179–182.

Joshi, J.B., Sharma, M.M., 1979. A circulation cell model for bubble columns. Transactions of the Institute of Chemical Engineers 57, 244–251.

Joshi, J.B., Veera, U.P., Prasad, C.V., Phanikumar, D.V., Deshphande, N.H., Thakre, S.S., Thorat, B.N., 1998. Gas holdup structure in bubble column reactors. PINSA 64 (4), 441–567.

Kastanec, F., Zahradnik, J., 1973. Gas–liquid reactors I. The residence time distribution in multistage bubble reactors. Collection Czechoslovia Chemical Communication 38, 3725–3741.

Kats, M.B., Genin, L.G., 1967. Study of longitudinal mixing of liquid in co-current sparged reactors sectionalized with sieve trays. International Chemical Engineering 7 (2), 246–252.

Kitai, A., Shinji, G., Ozaki, A., 1969. The performance of a perforated column as a multistage continuous fermentor. Journal of Fermentation Technology 47 (6), 340–347.

Levenspiel, O., 1972. Chemical Reaction Engineering. second ed. Wiley, New York.

Magnussen, P., Schumacher, V., 1978. Axial mixing of liquid in packed bubble columns and perforated plate columns of large diameter. Germany ACS Symposium Series, pp. 337–347.

Maretto, C., Krishna, R., 2000. Design and optimization of a multi-stage bubble column slurry reactor for Fischer–Tropsch synthesis. Third International Symposium on Catalysis in Multiphase Reactors, Naples, Italy, 29–31 May 2000.

Mills, P., Dudukovic, M., 1989. Convolution and deconvolution of non-ideal tracer response data with applications to three phase packed beds. Computers in Chemical Engineering 13 (8), 881–898.

Myers, K., 1986. Liquid-phase mixing in churn turbulent bubble columns. D.Sc. Thesis, Department of Chemical Engineering, Washington University, St. Louis, MO, USA.

Nauman, E.B., Buffham, B.A., 1983. Mixing in Continuous Flow Systems. Wiley, New York.

Palaskar, S.N., De, J.K., Pandit, A.B., 2000. Liquid phase RTD studies in sectionalized bubble column. Chemical Engineering Technology 23 (1), 61–69.

Patil, V.K., Joshi, J.B., Sharma, M., 1984. Sectionalized bubble column: gas holdup and wall side solid–liquid mass transfer coefficient. Canadian Journal of Chemical Engineering 62, 228–232.

Roemer, M., Durbin, L., 1967. Transient response and moments analysis of backflow cell model for flow systems with longitudinal mixing. I&E Fundamentals 6 (1), 120–129.

Schugerl, K., Todt, J., Lucke, J., Renken, A., 1977. Gas holdup and longitudinal dispersion in different types of multiphase reactors and their possible application for microbial processes. Chemical Engineering Science 32, 369–375.

Sekizawa, T., Kubota, H., 1974. Liquid mixing in multistage bubble column. Journal of Chemical Engineering Japan 7, 441–446.

Shah, Y.T., Kelkar, B.G., Godbole, S.P., Deckwer, W.D., 1982. Design parameters estimations for bubble column reactors. A.I.Ch.E. Journal 28 (3), 353–379.

Vinaya, M., 1994. Multistage bubble column, and liquid pulsed column. D.Sc. Thesis, Department of Chemical Engineering, Indian Institute of Technology, Madras, India.

Vinaya, M., Varma, Y.B.G., 1995. Some aspects of hydrodynamics in multistage bubble columns. Bioprocess Engineering 2, 231–237.